Electric Vehicles Charging Time Constrained Deliverable Provision of Secondary Frequency Regulation

Jinning Wang, *Graduate Student Member, IEEE*, Fangxing Li, *Fellow, IEEE*, Xin Fang, *Senior Member, IEEE*, Wenbo Wang, *Member, IEEE*, Hantao Cui, *Senior Member, IEEE*, Qiwei Zhang, *Member, IEEE*, and Buxin She, *Graduate Student Member, IEEE*

***Abstract*—Aggregation of electric vehicles (EVs) is a promising technique for providing secondary frequency regulation (SFR) in highly renewable energy-penetrated power systems. Equipped with energy storage devices, EV aggregation can provide reliable SFR. However, the main challenge is to guarantee reliable intra-interval SFR capacities and inter-interval delivery following the automatic generation control (AGC) signal. Furthermore, aggregated EV SFR provision will be further complicated by the EV charging time anxiety because SFR provision might extend EV's charging time. This paper proposes a deliverable EV SFR provision with a charging-time-constrained control strategy. First, a charging-time-constrained EV aggregation is proposed to address the uncertainty of EV capacity based on the state-space model considering the charging-time restriction of EV owners. Second, a real-time economic dispatch and time domain simulation (RTED-TDS) cosimulation framework is proposed to verify financial results and the dynamic performance of the EV SFR provision. Last, the proposed charging time-constrained EV aggregation is validated on the IEEE 39-bus system. The results demonstrate that with charging time-constrained EV aggregation, the dynamic performance of the system can be improved with a marginal increase in total cost. More importantly, the charging time constraint can be respected in the proposed SFR provision of the EV aggregation.**

***Index Terms*—Secondary frequency regulation, electric vehicle aggregation, charging time anxiety, state-space modeling, cosimulation.**

Manuscript received 10 April 2023; revised 11 September 2023 and 18 November 2023; accepted 16 January 2024. Date of publication 22 January 2024; date of current version 21 June 2024. This work was supported in part by CURENT, a National Science Foundation (NSF) Engineering Research Center funded by NSF and the Department of Energy under NSF Award EEC-1041877; in part by the Alliance for Sustainable Energy, LLC, the Manager and Operator of the National Renewable Energy Laboratory for the U.S. Department of Energy (DOE) under Contract DE-AC36-08GO28308; and in part by the U.S. Department of Energy Office of Electricity Grid Controls and Communications Program. Paper no. TSG-00528-2023. *(Corresponding author: Fangxing Li.)*

Jinning Wang, Fangxing Li, Qiwei Zhang, and Buxin She are with the Department of EECS, University of Tennessee, Knoxville, TN 37996 USA (e-mail: fli6@utk.edu).

Xin Fang is with the Department of Electrical and Computer Engineering, Mississippi State University, Mississippi State, MS 39762 USA.

Wenbo Wang is with the Grid Planning and Analysis Center, National Renewable Energy Laboratory, Golden, CO 80401 USA.

Hantao Cui is with the Department of Electrical and Computer Engineering, Oklahoma State University, Stillwater, OK 74077 USA.

Color versions of one or more figures in this article are available at https://doi.org/10.1109/TSG.2024.3356948.

Digital Object Identifier 10.1109/TSG.2024.3356948

NOMENCLATURE

Indices and Sets

Ω_B	Set of all buses
Ω_E	Set of all EV aggregators
Ω_G	Set of all generators
Ω_K	Set of all branches
Ω_T	Set of all RTED intervals

Parameters and Variables

$\Delta D_t^U/\Delta D_t^D$	Demanded RegUp/Dn capacity at time t
ρ_g^U/ρ_g^D	Ramp-up/-down limit (MW/min) of generator g
$c_{e,t}^U/c_{e,t}^D$	Price (\$/MWh) of EV aggregator g for RegUp/Dn at time t
$c_{g,t}$	Bid price (\$/MWh) of generator g at time t
$c_{g,t}^U/c_{g,t}^D$	Price (\$/MWh) of generator g for RegUp/Dn at time t
D_b	Load demand (MW) of bus b
$P_{g,t}^{\text{sch}}$	Scheduled power generation (MW) of generator g at time t
$P_{l,k}$	Line flow through branch k
$R_{e,t}^U/R_{e,t}^D$	RegUp/Dn capacity (MW) of EV aggregator e at time t
$R_{g,t}^U/R_{g,t}^D$	RegUp/Dn capacity (MW) of generator g at time t

I. INTRODUCTION

WITH the increasing integration of variable renewable energy generation involving solar power and wind power [1], [2], the stress confronted with system frequency regulation increases substantially. Secondary frequency regulation (SFR) is an essential grid service that maintains the power balance and regulates system frequency to its set value. To mitigate the fluctuation of the system frequency caused by variations in variable load and power generation, the SFR requirements increase significantly. However, given the gradual retirement of conventional generators, the controllable resources in the generation mix are continuously decreasing [3], [4]. Therefore, finding more alternative energy resources that can provide reliable SFR for the future power system with high-frequency regulation requirements is essential. Regarding the SFR, the ancillary market is generally

co-optimized with the energy market [5], [6] to maintain the intra-interval power balance. Once the procurement of SFR is settled down, the automatic generation control (AGC) units are responsible for delivering the intra-interval regulating power. Variable generation providing SFR brings the gap between the intra-interval procurement and the inter-interval delivery. Distributionally robust chance-constrained modeling is applied to obtain intra-interval SFR capacities and provide deliverable inter-interval SFR services [7].

Equipped with energy storage devices, Electric Vehicles (EV) can exchange power with the power grid in two directions to provide vehicle-to-grid services [8], [9], [10]. Since the capacity of a single EV is limited, the aggregation of a large population of EVs was developed to provide meaningful frequency service [11], [12], [13], [14]. The challenge of modeling EV aggregators is the randomness caused by numerous EVs' travel behaviors and heterogeneous parameters. An optimal dispatching control for EVs participating in LFC is developed to secure charging demand and enable dispatch level EV control [15]. EVs can be classified based on their SOC level and thus can be described as a Markov process and modeled as a state space transition model based on Markov theory [16], [17]. In addition, the communication burden is significantly reduced because the control signal is designed for groups rather than for every EV. However, the studies mentioned above focused on the continuous manner of AGC control while ignoring the SFR procurement and delivery process [7], [18], [19]. Additionally, charging anxiety, or named range anxiety [20], is a barrier that prevents EVs from participating in the SFR program because the energy consumed by the SFR will increase charging time. The problem of time anxiety is presented and alleviated by considering the patterns of EV behaviors [21]. In addition, the aggregated anxiety concept is proposed and a model-free deep reinforcement learning method is developed to optimize the charging schedule [22]. However, the methods discussed above are toward a single EV. They are not applicable in EVs that provide SFR because the relatively significant AGC power signal requires the aggregation of numerous EVs. However, the AGC action manner requires a near-real-time control. In summary, the challenges for EV providing SFR can be summarized as follows:

1) It should be addressed that EV randomness involves not only the procurement stage but also the delivery stage.
2) The increased charging time should be constrained to secure the preference of the EV owners.
3) The comprehensive evaluation of the SFR provision of EVs involves an economic perspective and dynamic performance.

Based on motivation, this paper proposes an increased charging time-constrained and deliverable SFR strategy from EVs. EV aggregation is modeled based on state-space modeling to effectively estimate the available SFR capacity in the procurement stage and reliably deliver the AGC signal in the real-time operation stage. Through the RTED-TDS cosimulation, the proposed strategy is validated to provide deliverable SFR service while the increased charging time is constrained to secure the EV owner's preference. The major contributions of this paper are summarized below:

1) The problem of EVs participating in the RTED to provide SFR is decoupled into dispatch modeling and EV aggregator modeling, where the procured capacity from EVs can be reliably delivered in the real-time operation stage to support current frequency regulation manner.
2) The increased charging time caused by the SFR services is translated into an action counter and is constrained by the EV owner's tolerance.
3) A hybrid OPF structure is proposed in the RTED-TDS cosimulation for frequency regulation studies, where the transition from dispatch to dynamic is secured and the modeling complexity is reduced. With the hybrid OPF structure, the proposed RTED-TDS cosimulation allows fast prototyping of dispatch-dynamic cosimulation studies.
4) EV providing deliverable SFR is verified using the proposed RTED-TDS cosimulation. The results show that the dynamic system performance is improved with the charging time constraints, and the EV owners' tolerance of increased charging time is obeyed.

The rest of this paper is organized as follows. Section II discusses the charging time-constrained EV aggregator modeling; Section III presents the problem formulation of EV providing SFR in the RTED and the framework of RTED-TDS cosimulation; Section IV verifies the proposed charging time-constrained EV control strategy using the proposed RTED-TDS cosimulation on the IEEE 39-bus system; and Section V concludes this paper.

II. Charging Time Constrained EV Aggregator Modeling

This section introduces the EV charging time-constrained aggregator model, including the estimation of SFR capacities in charge time and EV control for real-time AGC power delivery.

A. Overview State Space Model Based EV Aggregator

The uncertainties of EVs come from heterogeneous parameters and random travel behaviors. Various EV models provide heterogeneous parameters, including capacity Q, charging efficiency η_c, and discharging efficiency η_d. An EV must be plugged in if the SOC level reaches a low level after a trip, which consists of random traveling behaviors involving arrival time t_s, departure time t_f, initial SOC level SOC_i, and the SOC level required SOC_d.

A model-based EV aggregator based on the state space [23] is proposed to address the uncertainties of EV for frequency service. The proposed model applied the Markov state transition method to predict and control the aggregator status of the EV. Then, the power signals for EVs are translated to probabilities and acted by each single EV [17], [23], [24]. Here, we will overview the philosophy of the state space model-based EV aggregator.

An EV in a charging station can have three service actions, i.e., charging, idle, and discharging. Regulation services can be achieved by switching EVs between different statuses. Additionally, these EVs are categorized based on two criteria: SOC levels and charging behavior. SOC levels are grouped into N_s categories, while charging behaviors are described by three statuses: charging, idle, and discharging. Consequently, an individual EV can be assigned a status based on its SOC level and charging behavior. Additionally, all EVs can be collectively depicted using a $3N_s \times 1$ vector, where each element corresponds to a status partition. After a while, the EV will transition to a new state. Further, the status of a population of EVs can be described by a $3N_s \times 1$ vector that each element represents the proportion of EVs in a situation out of total EVs. Therefore, an EV population can be described with the state transition probability, as shown in Eqn. (1).

$$\begin{cases} \mathbf{x}(k+1) = \mathbf{A}(\mathbf{x}(k) + \mathbf{B}\mathbf{u}(k) + \mathbf{C}\mathbf{v}(k)) \\ y(k) = \mathbf{D}(\mathbf{x}(k) + \mathbf{B}\mathbf{u}(k) + \mathbf{C}\mathbf{v}(k)) \end{cases} \tag{1}$$

where vectors $\mathbf{x}(k)$ and $\mathbf{x}(k+1)$ are the $3N_s \times 1$ current and next state vectors corresponding to the proportion of each SOC, respectively, and $y(k)$ is the total output power of the EV aggregator.

The matrix $\mathbf{A}$ is the state transition matrix obtained by the estimation method or the analytical method [16]. Matrices $\mathbf{B}$ and $\mathbf{C}$ are the constant matrices corresponding to the control signals of RegUp and RegDn, as given in Eq. (2)-(3). The vectors $\mathbf{u}$ and $\mathbf{v}$ are the input vectors $N_s \times 1$ that corresponds to the proportion of each SOC. A positive element in $\mathbf{u}$ means that the EV aggregator will switch part of the EVs to the corresponding charging state. On the contrary, the negative element means that the EV changes from idle to charging. Similarly, a positive element in $\mathbf{v}$ means that part or all EVs in the corresponding state will be switched from idle to charging. In contrast, the negative element means changing from discharging to idle. The calculation of $\mathbf{u}$ and $\mathbf{v}$ is discussed in the next subsection:

$$\mathbf{B} = \left[-\mathbf{I}_{1\times N_s}, \mathbf{I}_{1\times N_s}, \mathbf{0}_{1\times N_s}\right]^T \tag{2}$$

$$\mathbf{C} = \left[\mathbf{0}_{1\times N_s}, -\mathbf{I}_{1\times N_s}, \mathbf{I}_{1\times N_s}\right]^T \tag{3}$$

The matrix $\mathbf{D}$ is the constant matrix corresponding to the output power as given in Eqn. (4).

$$\mathbf{D} = P_{\text{ave}} N_e \left[-\mathbf{1}_{1\times N_s}, \mathbf{0}_{1\times N_s}, \mathbf{1}_{1\times N_s}\right] \tag{4}$$

where N_e is the online EV numbers and P_{ave} is the estimated average charging power of the EVs. N_e and P_{ave} can be obtained from the EV charging station operation history data, and the computation error can be bounded by periodically updating [16].

Further, the upper and lower bound of the EV aggregator power can be described below:

$$\begin{cases} \overline{y(k)} = P_{\text{ave}} N_e \cdot \mathbf{1}_{3\times N_s} \cdot \mathbf{x}(k) \\ \underline{y(k)} = -P_{\text{ave}} N_e \cdot \mathbf{1}_{3\times N_s} \cdot \mathbf{x}(k) \end{cases} \tag{5}$$

With state space modeling, control signal computation, and communication are significantly simplified because the EV aggregator deals with a state vector of a large population of EVs rather than every single EV.

TABLE I
AGC POWER FROM SINGLE EV

P_r \ Status / SOC	Charging	Idle	Discharging
$SOC < SOC_d$	0	P_u	$2P_u$
$SOC \geq SOC_d$	$-P_u$	0	P_u

B. Charging Time Constrained SFR Capacities Estimation

Charging time anxiety of EV has drawn interest [20], [21], [22], the increased charging time incurred by the AGC response can impede electric vehicle owners participating in SFR program. Therefore, the charging time should be considered to follow the EV owners' tolerance to the increased charging time.

When a large electric vehicle population is plugged in, there can be a gap between the energy demanded and the charging energy during the charging period. As a result, the gap allows electric vehicles to provide frequency regulation services without increasing charging time. For a single EV, Eqn. (6) describes the energy available for frequency support that secures the EV owner's charging anxiety, where t_{tol} is the EV owner's tolerance of increased charging time:

$$E_a = \left(t_f - t_s + t_{\text{tol}}\right) \cdot P_c - (SOC_d - SOC_i) \cdot Q \tag{6}$$

Given the condition that the departure time t_f is challenging to access in practice, Eqn. (6) can be further revised for the EV aggregator application,

$$E_a' = \left(t_{\text{stay,ave}} + t_{\text{tol}}\right) \cdot P_{\text{ave}} - (SOC_d - SOC_i) \cdot Q_{\text{ave}} \tag{7}$$

where $t_{\text{stay,ave}}$ is the average time of EV staying connected in the charging station, and Q_{ave} is the average capacity. Similar to P_{ave} [16], $t_{\text{stay,ave}}$ and Q_{ave} can also be obtained from the operation data of the EV charging station, as shown in Eqns (8)–(9), where $f_t(t_c)$ and $f_Q(Q_c)$ are the probability density functions of t_{stay} and Q, respectively; $t_{c,\min}$ and $t_{c,\max}$ are the minimum and maximum stay time, respectively; $Q_{\min}$ and $Q_{\max}$ are the minimum and maximum capacity, respectively.

$$t_{\text{stay, ave}} = \int_{t_{\text{stay,min}}}^{t_{\text{c, max}}} t_c \cdot f_t(t_c)\, dt_c \tag{8}$$

$$Q_{\text{ave}} = \int_{Q_{\min}}^{Q_{\max}} Q_c \cdot f_Q(Q_c)\, dQ_c \tag{9}$$

Before integrating the charging time constraints, the assumptions for EV in this study are listed below:

- An EV is set to charging status when it connects to the charger.
- The EV owner will input the charge time tolerance t_{tol} into the charger.
- The EV owner will input the SOC level of demand SOC_d into the charger.
- The EV will be switched to idle status if it has been charged to the demand SOC level.
- The EV will remain unchanged if switch failure happened due to communication error or chip malfunction.

Since the time length of the AGC interval is fixed, the response power P_r from a single EV in an AGC interval is listed in Table I. In it, $P_u = P_{\text{ave}} \cdot T_{\text{agc}}$ is the unit power of AGC response from one single EV during an AGC interval, and T_{agc} is the AGC cycle time. EVs that have not been charged to SOC_d are supposed to be in charging status; thus, the EVs in idle and discharging status are considered to be providing AGC response power. Similarly, EVs charged to SOC_d are supposed to be idle; thus, the EVs in charging and discharging status are considered to provide AGC response power.

Eqn. (10) translates the available energy E'_a into $\overline{N_a}$, an action number limit of AGC response. Here, the variable $\overline{N_a}$ is an integer obtained through the floor operation. Regarding the application of superchargers, which introduce a variety of charging rates, the proposed model can be extended to encompass this as discussed in [17]. For an individual EV, N_a is initially set to zero upon its arrival at the charging station. The counter is updated after every AGC interval by $N_a = N_a + P_r/P_u$, and once the maximum action number is reached, the EV will be out of SFR service. Similarly, an EV will also exit the SFR service if it attains a full charge. This strategy ensures that the EV does not remain in the service, guarding against the risk of overcharging and maintaining optimal battery health. Note that Eqns. (7) and (10) use estimated t_{tol}, P_{ave}, and Q_{ave} to calculate the action limiter of an individual EV, ensuring the charging demand. In practice, an EV charger could access more accurate data, which would improve the estimations:

$$\overline{N_a} = \lfloor \frac{E'_a}{P_{\text{ave}} \cdot T_{\text{agc}}} \rfloor \tag{10}$$

In this way, the charging time constraints can be realized by installing a counter locally in each charger, and thus there is no extra communication burden between the charging center and the charger. In addition, the increased charging time can be estimated by the counter as $t_{\text{ICT}} = N_a/\overline{N_a}$.

Then, the number of online EVs N_e in Eqns. (4)-(5) should be replaced with N_c, which represents the number of in-service EVs.

Further, the charging time-constrained SFR capacities can be estimated by Eqn. (11):

$$\begin{cases} \overline{R_e^U} = \overline{y_{(k)}} - y(k) \\ \overline{R_e^D} = y(k) - \underline{y_{(k)}} \end{cases} \tag{11}$$

where $\overline{R_e^U}$ and $\overline{R_e^D}$ are the estimated RegUp and RegDn capacities from the EV aggregator, respectively.

C. Real-Time AGC Power Delivery Control

EV aggregator participates in the SFR in two stages: dispatch in RTED and real-time delivery in real-time. By Eqn. (11), the power grid control center can procure the regulation capacities from EV as discussed in Section III-A. Then, in the real-time operation, the EV aggregator delivers the assigned signal. The real-time AGC power delivery is illustrated below:

1) The power signals for each status of the EV are computed as follows:

If $P_{\text{ev}} - P_{\text{rt}} \geq 0$:

$$\begin{cases} r_u = min\Big(P_i,\ \overline{R_e^U}\Big)/(P_{\text{ave}} \cdot N_c) \\ u_j = min\Big(r_u - \sum_{h=j+1}^{N_s} x_h - \sum_{h=j+1+N_s}^{2N_s} x_h,\ x_j\Big) \\ r_v = max\Big(P_i - \overline{R_e^U},\ 0\Big)/(P_{\text{ave}} \cdot N_c) \\ v_j = min\Big(r_v - \sum_{h=j+1}^{N_s} (x_{h+N_s} + u_h),\ x_{j+N_s} + u_j\Big) \end{cases} \tag{12}$$

Else if $P_{\text{ev}} - P_{\text{rt}} < 0$:

$$\begin{cases} r_v = max\Big(P_i,\ \overline{R_e^D}\Big)/(P_{\text{ave}} \cdot N_c) \\ v_j = max\Big(r_v + \sum_{h=1}^{j-1} (x_{h-1+2N_s}),\ -x_{j+2N_s}\Big) \\ r_u = min\Big(P_i - \overline{R_e^D},\ 0\Big)/(P_{\text{ave}} \cdot N_c) \\ u_j = max\Big(r_u - \sum_{h=1}^{j} v_h - \sum_{h=1}^{j-1} u_h,\ -x_{j+N_s}\Big) \end{cases} \tag{13}$$

where $j = [1, \ldots, N_s]$, P_{ev} is the AGC power assigned to the EV aggregator, P_{rt} is the AGC power from the EV aggregator that can be summarized from all the response power P_r from every single EV as listed in the Table I, x is the single element in vector $\mathbf{x}$, x_{h+N_s} is the element in vector $\mathbf{x}$ that represents for EVs in SOC level h at idle status, x_{j+N_s} is the element in vector $\mathbf{x}$ that represents for EVs in SOC level j at idle status.

2) The power signals for each EV status are translated into probabilities as follows:

If $P_{\text{ev}} - P_{\text{rt}} \geq 0$:

$$\begin{cases} u_{s,j} = min\big(u_j/x_j,\ 1\big) \\ v_{s,j} = min\big(v_j/(x_{j+N_s} + u_j),\ 1\big) \end{cases} \tag{14}$$

Else if $P_{\text{ev}} - P_{\text{rt}} < 0$:

$$\begin{cases} v_{s,j} = min\big(-v_j/(x_{j+2N_s} + u_j),\ 1\big) \\ u_{s,j} = min\big(-u_j/x_{j+N_s} - v_j,\ 1\big) \end{cases} \tag{15}$$

where x_{j+N_s} is the element in vector $\mathbf{x}$ that represents for EVs in SOC level j at idle status, and x_{j+2N_s} is the element in vector $\mathbf{x}$ that represents for EVs in SOC level j at discharging status.

In Eqns. (12) and (14), RegUp power is delivered by EVs that will be switched from idle to discharging and by EVs that will be switched from charging to idle. RegUp power delivered by EVs switching from idle to discharging is associated with r_u, u_j, and $u_{s,j}$. These represent the total assigned power, the power assigned to EVs in SOC level j, and the switch probability assigned to EVs in SOC level j, respectively. RegUp power delivered by EVs switching from charging to idle is linked to r_v, v_j, and $v_{s,j}$. These denote the total assigned power, the power assigned to EVs in SOC level j, and the switch probability assigned to EVs in SOC level j, respectively.

In Eqns. (13) and (15), RegDn power is delivered by EVs that will be switched from discharging to idle and by EVs that will be switched from idle to charging. RegDn power delivered by EVs switching from discharging to idle is associated with r_v, v_j, and $v_{s,j}$. These represent the total assigned power, the power assigned to EVs in SOC level j, and the switch probability assigned to EVs in SOC level j, respectively. RegDn power delivered by EVs switching from idle to charging is linked to r_u, u_j, and $u_{s,j}$. These denote the total assigned power, the power assigned to EVs in SOC

Algorithm 1 EV Aggregator Control

```
Initialize EV aggregator
for t in T_total
    if t = N · T_ed
        Estimate SFR capacities with Eqn. (11);
    if t = N · T_p
        Record x and update A;
    if t = N · T_agc
        Compute signals with Eqns. (12)-(16);
    Run Monte Carlo simulation;
    Switch EVs with Eqn. (17);
    Estimate x and y with Eqn. (1);
```

level j, and the switch probability assigned to EVs in SOC level j, respectively.

3) The probabilities signals from 2) are supplemented with direction signals as the following:

$$\begin{cases} u_{s,N_{s+1}} = v_{s,N_{s+1}} = 1, \ P_{\text{ev}} - P_{\text{rt}} \geq 0 \\ u_{s,N_{s+1}} = v_{s,N_{s+1}} = -1, \ P_{\text{ev}} - P_{\text{rt}} < 0 \end{cases} \tag{16}$$

4) The signals from Eqns. (14)-(16) are broadcast to all the EVs, and each single EV will generate a number n locally, where $n \sim U(0, 1)$. The action is then determined by comparing the number n with the corresponding status p:

$$\begin{cases} \text{switch}, \ n \geq p \\ \text{stay}, \ n < p \end{cases} \tag{17}$$

The overall workflow of the EV aggregator is summarized in the Algorithm 1, where $N \in N_0$, T_{ed} is the cycle time of RTED and T_p is the update cycle time of EV aggregator.

III. Procurement and Delivery of SFR From EV

This section introduces the procurement of EV SFR capacity in the RTED and the RTED-TDS cosimulation framework used to verify the proposed strategy.

A. Procurement of EV SFR in the RTED

The procurement of EV SFR ($R^U_{e,t}$ and $R^D_{e,t}$) in the RTED requires the EV aggregator to provide available SFR capacities $\overline{R^U_e}$ and $\overline{R^D_e}$. Given the EV aggregator addresses the EV uncertainties, the RTED can be modeled as below, where the variables are explained in the Nomenclature:

$$\min \sum_{t\in\Omega_T}\left(\sum_{i\in\Omega_G}\left(f_{g,t}\left(P^{\text{sch}}_{g,t}\right) + c^U_{g,t}R^U_{g,t} + c^D_{g,t}R^D_{g,t}\right) + \sum_{i\in\Omega_E}\left(c^U_{e,t}R^U_{e,t} + c^D_{e,t}R^D_{e,t}\right)\right), \forall g \in \Omega_G, \forall e \in \Omega_E \tag{18}$$

s.t.

$$\Delta D^U_t = \sum_{g\in\Omega_G} R^U_{g,t} + \sum_{e\in\Omega_E} R^U_{e,t} \tag{19}$$

$$\Delta D^D_t = \sum_{g\in\Omega_G} R^D_{g,t} + \sum_{e\in\Omega_E} R^D_{e,t} \tag{20}$$

$$\sum_{b\in\Omega_B} P^{\text{sch}}_{g,t} - \sum_{b\in\Omega_B} D_b = 0 \tag{21}$$

$$P^{\text{sch}}_{g,t} + R^U_{g,t} \leq \overline{P_g}, \forall g \in \Omega_G, \forall t \in \Omega_T \tag{22}$$

$$\underline{P_g} \leq P^{\text{sch}}_{g,t} - R^D_{g,t}, \forall g \in \Omega_G, \forall t \in \Omega_T \tag{23}$$

$$R^U_{e,t} \leq \overline{R^U_e}, \forall e \in \Omega_E, \forall t \in \Omega_T \tag{24}$$

$$R^D_{e,t} \leq \overline{R^D_e}, \forall e \in \Omega_E, \forall t \in \Omega_T \tag{25}$$

$$P_{g,t} - P_{g,t-1} \leq \rho^U_g \cdot \Delta t, \forall i \in \Omega_G, \forall t \in \Omega_T \tag{26}$$

$$P_{g,t-1} - P_{g,t} \leq \rho^D_g \cdot \Delta t, \forall i \in \Omega_G, \forall t \in \Omega_T \tag{27}$$

$$-\overline{P_{l,k}} \leq \sum_{g\in\Omega_G} GSF_{g,k}\left(P^{\text{sch}}_{g,t} - D_g\right) \leq \overline{P_{l,k}}, \forall k \in \Omega_K \tag{28}$$

The underline and overline of the variables represent the minimum and maximum, respectively. Superscripts U and D represent regulation up and down, respectively. Eqn. (18) is the objective function; Eqns. (19)–(20) represent the SFR equality constraints; Eqn. (21) represents the power balance; Eqns. (22)–(23) are the minimum/maximum output of conventional units; Eqns. (24)–(25) is the minimum/maximum SFR output of the EV aggregator, where the $R^U_{e,t}$ and $R^D_{e,t}$ are estimated from the EV aggregator as described in the previous Section II-C; Eqns. (26)–(27) are the ramping up/down limits of conventional units; Eqn. (28) represents the line thermal limits, where $\overline{P_{l,k}}$ is the thermal limit of line k and $GSF_{g,k}$ is generation shift factor of bus g to line k. In the RTED modeling, the decision variables are $P^{\text{sch}}_{g,t}$, $R^U_{g,t}$, $R^D_{g,t}$, $R^U_{e,t}$, $R^D_{e,t}$.

Once the SFR capacities are settled down, the participation factor of each AGC unit is determined by the ratio of its SFR capacity out of the total demanded SFR capacity, as shown in Eqns. (29)-(30):

$$\beta^U_{g,t} = R^U_{g,t}/\Delta D^U_t, \forall g \in \Omega_G \cup \Omega_E, \forall t \in \Omega_T \tag{29}$$

$$\beta^D_{g,t} = R^D_{g,t}/\Delta D^D_t, \forall g \in \Omega_G \cup \Omega_E, \forall t \in \Omega_T \tag{30}$$

where the $\beta^U_{g,t}$ and $\beta^D_{g,t}$ are each AGC unit's RegUp and RegDn participation factors, respectively.

B. RTED-TDS Cosimulation Framework

RTED-TDS cosimulation is proposed to simulate the close-loop AGC control on the area level. The complete frequency regulation study includes the dispatch results and the dynamic process. However, there can be a gap when applying the RTED solution to the TDS. In the RTED-related problem formulation, DCOPF or the linearized ACOPF can be used, while the ACOPF is used to initialize the TDS. The gap results from DCOPF or linearized ACOPF will result the slack generator will compensate for the unbalanced power. Thus, scheduling results can be broken and TDS can fail. Therefore, to reduce the modeling complexity and guarantee a smooth transition from dispatch to dynamic, a DC-AC hybrid OPF structure is proposed. The design of DCOPF and ACOPF hybrid solutions allows the extensibility to other dispatch formulations, such as unit commitment problems. In this design, DCOPF enables rapid prototyping of dispatch problems, while ACOPF secures the consistency and initialization of the TDS.

Figure 1 illustrates the proposed framework of RTED-TDS cosimulation. The framework coordinates four entities: EV

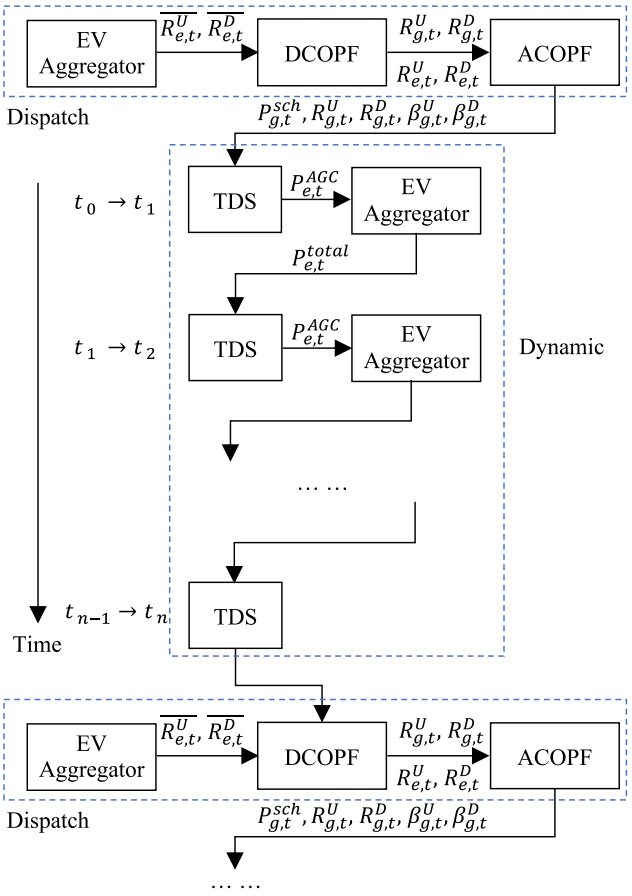

Fig. 1. Framework of RTED-TDS cosimulation.

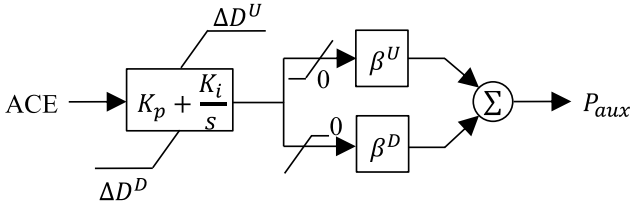

Fig. 2. AGC unit control.

Aggregator is the proposed charging time-constrained EV aggregator, DCOPF stands for the DCOPF-based dispatch simulator, ACOPF represents the ACOPF-based dispatch simulator, and TDS is the dynamic simulator. The dispatch simulator involves the DCOPF, and ACOPF implemented with gurobipy and pandapower [25], respectively. The dynamic simulation is powered by the open-source simulation engine LTB ANDES [26], [27]. To capture the EV dynamics, the data is federated between the EV aggregator and the dynamic model [28]. The four entities are grouped into two modules, i.e., dispatch and dynamic, and the two modules are iterated to perform the cosimulation.

The dispatch module contains three steps. First, the available SFR capacities from the EV aggregator and other AGC units are reported to the control center. Second, the procurement of SFR ($R^U_{g,t}$, $R^D_{g,t}$, $R^U_{e,t}$, $R^D_{e,t}$) is solved with DCOPF-based RTED model as described in Section III-A. However, the setting points $P^{\text{sch}}_{g,t}$ solved from DCOPF can result in a mismatch in the TDS. Third, therefore, setting points $P^{\text{sch}}_{g,t}$ are re-solved from ACOPF to secure the initialization of TDS and the accuracy of the dispatch results. The SFR capacities and the ramping limits from the first step are reserved by adjusting the generator limits, as shown in Eqns. (31)-(32).

$$\overline{P'_g} = min\left(\overline{P_g} - R^U_{g,t}, \overline{P_g} - \rho^U_g \cdot \Delta t\right) \tag{31}$$

$$\underline{P'_g} = max\left(\underline{P_g} + R^D_{g,t}, \underline{P_g} + \rho^U_g \cdot \Delta t\right) \tag{32}$$

Once the dispatch results are settled, the dynamic module will run the TDS by iterating ANDES and the EV aggregator. The iteration involves two steps. First, the TDS will run to set end time $t_{0,0}$ and generate the AGC signal $P^{\text{AGC}}_{e,t}$ of the EV aggregator. Second, the EV aggregator responds to the AGC signal while running to the same end time $t_{0,0}$. Then the two steps are iterated till the end of the first dynamic period.

After the dynamic simulation, the dynamic results will be reported to the control center as the start point in the following dispatch period.

The secondary frequency regulation on the area level is implemented in the area-level area control error (ACE) model and the plant-level automatic generation control (AGC) model. The area-level ACE represents the system power imbalance and is defined by North America Electric Reliability Corporation [1]. With the ignorance of interchange (tie line) metering error, it can be calculated with Eqn. (33), where β is the system bias factor (MW/0.1Hz), f and f_n are the measured and nominal frequency (Hz), respectively, P_{tl} and $P^{\text{sch}}_{\text{tl}}$ are the actual tie line power (MW) and the scheduled tie line power (MW), respectively.

$$ACE = 10\beta(f - f_n) + \left(P_{\text{tl}} - P^{\text{sch}}_{\text{tl}}\right) \tag{33}$$

Taking ACE as the input signal, the plant-level AGC model will generate auxiliary power signal P_{aux}, as illustrated in Figure 2, where K_p and K_i are the gain and integral constants of the PI controller, respectively.

In the power system operation, the SFR mileage calculation must be necessary. The actual SFR mileages of EV aggregator are similar to conventional generators, as given in Eqn. (34):

$$P_{\text{mile},i_{\text{ed}}} = \sum_{i_{\text{agc}}=1}^{N_{\text{agc}}-1} |P_{\text{agc},i_{\text{agc}}+1,i_{\text{ed}}} - P_{\text{agc},i_{\text{agc}},i_{\text{ed}}}| \tag{34}$$

where $P_{\text{mile},i_{\text{ed}}}$ is the mileage of EV aggregator of the $i_{\text{ed}}th$ RTED interval, $P_{\text{agc},i_{\text{agc}},i_{\text{ed}}}$ means the AGC power of EV aggregator of the $i_{\text{agc}}th$ AGC interval in the $i_{\text{ed}}th$ RTED interval.

As illustrated in the Algorithm 2, lines 4–8 are the dispatch module, and lines 10–14 are the dynamic module. The detailed data federation is listed below:

1) line 4: the available SFR capacities from EV are computed with Eqn. (11) and updated into Eqns. (25)-(24) of TDS;
2) line 6: the previous setting points P^{t-1}_g of Eqns. (22)-(23) of TDS are replaced with actual output power from TDS results;

Algorithm 2 RTED-TDS Cosimulation

```
1: Initialize EV aggregator, DCOPF, ACOPF, TDS
2: for t in T_total
3:     if t = N · T_ed
4:         EV aggregator: estimate SFR with Eqn. (11);
5:         DCOPF: update info from dynamic;
6:                solve RTED with Eqns. (18)-(30);
7:         ACOPF: resolve with Eqns. (31)-(32);
8:         TDS: assign schedule results from ACOPF;
9:     if t = N · T_agc
10:        TDS: assign AGC power;
11:        EV Aggregator: run with Algorithm 1;
12:    TDS: federate power from EV aggregator;
13:            run TDS;
14:            compute ACE with Eqn. (33);
```

3) line 8 the setting points calculated from ACOPF are updated into corresponding generation units in TDS;
4) line 12: the output power of the EV Aggregator is updated into the EV dynamic model in TDS.

IV. Case Studies

For verification and demonstration, this section carries out case studies using the proposed RTED-TDS cosimulation. The IEEE 39-bus system is modified to demonstrate the potential of EVs participating in SFR with the proposed charging time-constrained aggregator modeling.

A. Simulation Settings

All studies are performed on a laptop with Apple M1 processors and 16 GB RAM. The environment of the EV aggregation algorithm and the RTED-TDS cosimulation is deployed in Python 3.9 with LTB ANDES 1.7.

The EV parameters are randomly generated according to a given distribution [16], and detailed EV profiles are simulated with the EV aggregator. In the EV aggregator, Monte Carlo simulation is conducted by updating EV connection status and SOC at each time step, as outlined in Algorithm 1. The EV aggregator parameters are set as follows: step size $T_e = 1s$, SOC intervals $N_s = 20$, and update cycle $T_p = 40s$. The step size of the cosimulation is set as $T_c = 1s$. The heaviest charging load occurs around 6 PM [23], and the average SOC level is relatively lower than in other time intervals. Thus, the scenario at 6 PM is chosen to demonstrate the secured charging demand and the potential of aggregated EVs participating in SFR provision with charging time constraints.

The load profile is synthesized from PJM load data [29], as depicted in Figure 3.

B. EV Aggregator Modeling Validation

In the TDS, there are two approaches to modeling EV dynamics. First, we can model every EV to secure the simulation accuracy, marked as M1. However, this detailed modeling in M1 can bring a heavy computation burden when the EV number is significant. To address this issue, the second approach is to aggregate the large number of EVs into one single dynamic EV device, with the output power set to track the total output power of all EVs, marked as M2. Note that, with the aggregated M2, although some details, such as each EV's SOC and output power, are excluded in the TDS, these detailed individual EV operational parameters are calculated in the separated EV aggregator model.

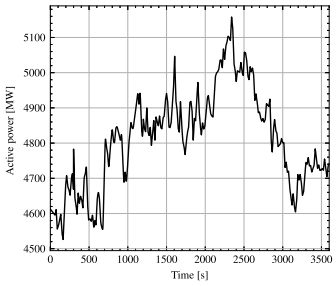

Fig. 3. System load curve.

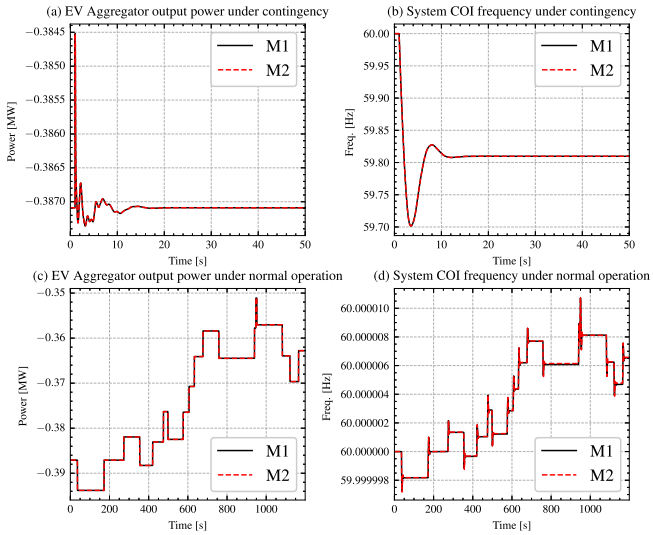

Fig. 4. Benchmark of EV modeling (a) Total power under normal operation; (b) System frequency under normal operation; (c) Total power under generator tripping; (d) System frequency under generator tripping.

IEEE 39-bus system with EV dynamic devices is used to validate the accuracy of the M2 model. In the benchmark test, M1 includes all the 1,000 EV dynamic devices in the TDS, while M2 only contains one.

The 50s simulation under a generation trip contingency consumes 3.400s using M1 versus 2.237s using M2. The 1200s simulation under regular operation consumes 895s using M1 versus 172s using M2. Figure 4 shows the system's dynamic responses. From the above results, it can be seen that M2 significantly accelerates the simulation while reserving EV information with high accuracy. Therefore, M2 is used in this study to investigate the aggregated EV providing SFR.

C. IEEE 39-Bus System

As visualized using LTB AGVis [30] in Figure 5, IEEE 39-bus system is modified to include an EV aggregator with a total of 50,000 EVs.

TABLE II
IEEE 39-BUS SYSTEM GENERATION PARAMETERS

Unit	Cost ($/MW)				Pmax (MW)	Pmin (MW)	Ramp (MW/5 min)
	a	b	c	SFR			
G1	0.0140	20	500	0	10.4	4.16	52
G2	0.0200	20	380	0	6.46	2.58	40
G3	0.0194	20	42	0	7.25	2.9	43.33
G4	0.0200	20	380	0	6.52	2.6	36.67
G5	0.0255	20	295	0	5.08	2.0	26.67
G6	0.0210	20	400	0	6.87	2.74	35
G7	0.2300	20	350	0	5.8	2.32	30
G8	0.2220	20	330	0	5.64	2.256	30
G9	0.0150	20	490	0	8.65	3.64	50
G10	0.1400	20	500	0	11	4.4	66.67

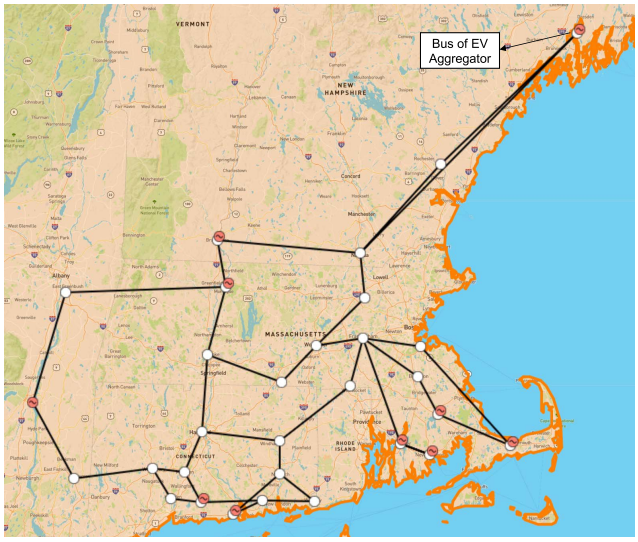

Fig. 5. IEEE 39-bus system topology visualized by LTB AGVis.

The generation parameters [31] are listed in Table II. Referenced from ISO-NE, the mileage price is set as 0.99$/MWh, and the penalty of extra increased charging time is set as 4$/h. Three cases listed below are tested to demonstrate the charging time-constrained EV aggregator modeling:

- Case1: EV not providing SFR
- Case2: EV providing SFR without charging time constraints
- Case3: EV providing SFR with charging time constraints

The simulation results are shown and interpreted in the following subsections.

D. EV Aggregator Results

Figure 6 illustrates the EV Aggregator response of Case2 and Case3. It can be seen that the AGC power assigned to the EV aggregator is delivered accurately. Noted that Case1 is not included in Figure 6 because Case1 EV aggregator has zero control and response signal. This is also the case for Figure 7 and 9.

Although the recent developments in 5G technology could offer a practical solution for the proposed EV aggregator [32],

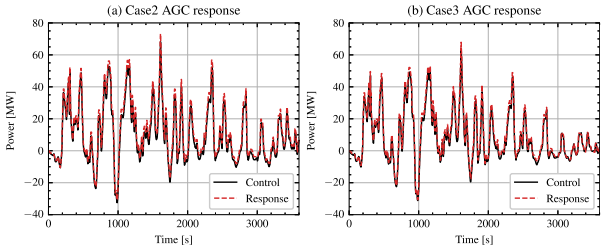

Fig. 6. EV aggregator response.

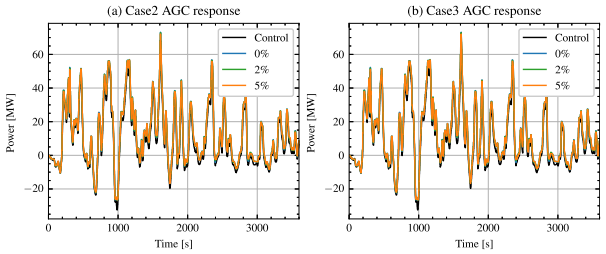

Fig. 7. EV aggregator response with communication failure.

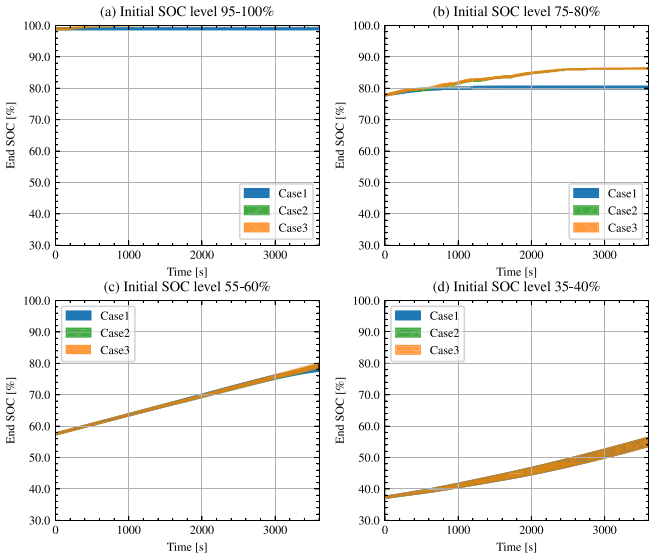

Fig. 8. 95% confidence interval of ended SOC by a group of initial SOC.

real-world scenarios encompass practical conditions, including communication errors or chip malfunctions, which can lead to switch failures in EV chargers. Consequently, these factors can compromise the regulation performance of the EV aggregator. Figure 7 presents the AGC responses of the EV aggregator under varying failure rates. The figure portrays both the AGC responses of the EV aggregator with and without the increased charging time control. Here, the control signal in Case 2 is used as EV aggregator input signal for all three scenarios. The black curve represents the input signal, while the blue, green, and orange curves correspond to 0%, 2%, and 5% failure rate, respectively. From the figure, it can be seen that the AGC responses for different failure rates closely follow the control signal and exhibit similar patterns. The robustness comes from that the large number of EVs contributes to upholding overall performance at an acceptable level, even in cases where a limited number of individual EVs fail to act as expected.

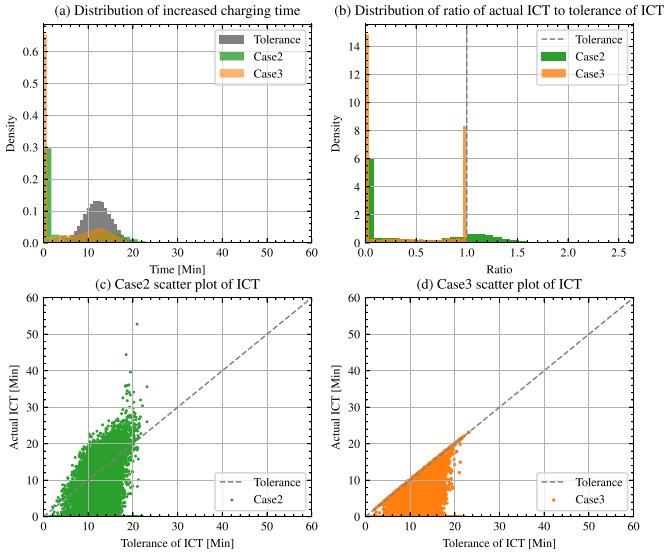

Fig. 9. EV increased charging time.

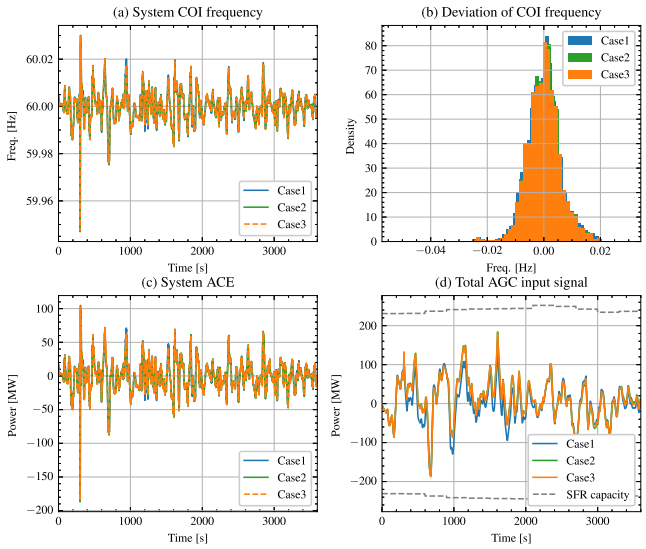

Fig. 10. System dynamic results.

Figure 8 depicts the 95% confidence interval of the EV SOC curve by four groups of different initial levels of SOC. In Figure 8 (a) and (b), EVs that have been charged to the desired SOC level are still charged in Case2 and Case3, whereas in Case1, they remained unchanged. RegDn power is withdrawn from switching idle EVs to charging, where EVs already charged to demanded SOC are usually idle. When comparing Figures 8(c) and (d) with (a) and (b), it can be seen that the control strategy can ensure the charging demand of EVs with lower initial SOC levels. Figure 8 shows that the EV aggregator control strategy can secure EV charging demand.

Figure 9 illustrates the increased charging time of Case2 and Case3. In Figure 9(a), the distribution shape of Case3 is similar to that of the tolerance, while Case2 is out of the tolerance range. Additionally, Figure 9 (b) shows the ratio of increased charging time to tolerance for every EV. In Case 2, parts of EVs exceed the tolerance, while the tolerance in Case 3 limits the increased charging times. In addition, the scatter plots of increased charging time in Figure 9(c) and (d) show again that the tolerance of increased charging time is violated in Case2 but obeyed in Case3. Figure 9 verifies that the tolerance of charging time constraints is followed well by using the proposed charging time constraints.

In summary, Figure 6 demonstrates the EV aggregator's dynamic performance in accurately delivering power signals. Figure 7 confirms method robustness under varied failure rates, supported by numerous EVs. Figure 8 highlights successful charging time constraint application, while Figure 9 validates charging time adherence. This approach not only confirms dynamic performance but also sustains charging time constraints.

E. System Results

Figure 10 shows the dynamic results of the system. Figure 10 (a) illustrates the COI frequency of the system. The spikes of Case2 and Case3 are slightly lower than those of Case1, but Case2 and Case3 overlap almost. A similar condition can be seen from the distribution of the COI frequency as shown in Figure 10(b). The distribution of the COI frequency deviation is more concentrated in Case2 and Case3 than in Case1, and the variation is slightly more concentrated in Case3 than in Case2. Figure 10(c) shows the system ACE. This figure is similar to Figure 10(a) because the test system is controlled as one area. Figure 10 (d) shows the total AGC input signal of the system, where the dashed lines represent the SFR capacity. The figure indicates that the SFR capacities are sufficient in all three test cases. However, when comparing Case2 and Case3 versus Case1, it can be found that when the EV provides SFR, the system assigns more RegDn power while less RegUp power.

TABLE III
SYSTEM FREQUENCY REGULATION METRICS

	Case1	Case2	Case3
Freq. Dev. mean [Hz]	0	0.00001	0.00001
Freq. Dev. Std. [Hz]	0.00623	0.00600	0.00603
ACE mean [MW]	-0.01521	-0.0522	-0.03912
ACE Std. [MW]	21.78	20.98	21.07
CPS1 score	153.09	156.71	156.26
AGC mileage [MWh]	8277.80	8940.77	8864.53
EV AGC mileage[MWh]	0	2043.34	1801.42

To be more specific, Table III shows the metrics of system frequency regulation. When looking at the CPS1 score, it can be found that EV providing SFR enhances the CPS1 score by comparing Case2 and Case3 versus Case1. In addition, Case2 and Case3 consumed more AGC mileage than Case1. Comparing Case2 versus Case3 shows that their dynamic performance is close, although, in Case3, the charging time constraints slightly degraded the frequency metrics. In summary, Table III indicates that EV providing SFR slightly enhanced the system dynamic performance while consuming more AGC mileage. The charging time constraints of EV aggregators bring a few impacts on the system's dynamic performance.

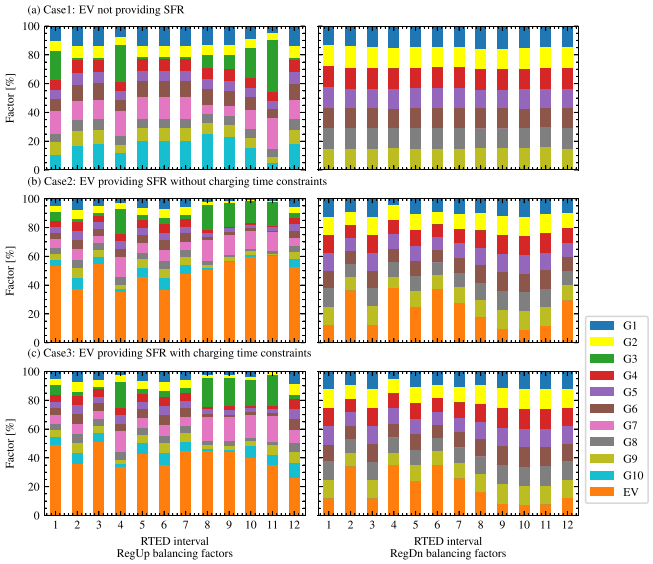

Fig. 11. System balancing factors.

TABLE IV
SYSTEM ECONOMIC RESULTS

	Case1	Case2	Case3
Generation cost [$]	133,031	132,501	132,556
Mileage payment [$]	8,195	8,851	8,776
Mileage payment to EV [$]	0	2,023	1,783
ICT compensation to EV [$]	0	846	0
System total cost [$]	141,226	142,198	141,332

The balancing factors of the three cases are illustrated in Figure 11. When comparing Case2 and Case3, it can be seen that the balancing factors of the EV aggregator in Case3 are lower than those of Case2 for both RegUp and RegDn. This indicated that the charging time constraints resulted in a decrease in frequency regulation capacities.

Table IV shows the system's economic results. When comparing Case2 and Case3 versus Case1, it can be seen that EV-providing SFR reduces the system generation cost. This is caused by the decreased load from the EV charging station when EV provides SFR. Consistent with AGC mileage in Table III, EV participating SFR results in higher mileage payment, and the mileage payment of Case3 is close to Case2. Regarding the compensation for extra increased charging time, by comparing Case 2 versus Case 3, it should be noticed that there is almost zero compensation in Case 3. Further, the system total cost shows that Case3 is lower than Case2 while close to Case1. Table IV implies that EV aggregators with charging time constraints have limited impacts on the system's economic performance.

The Case Studies demonstrate the benefits of charging time-constrained EV aggregation providing SFR. First, the reliable real-time delivery of the EV aggregator proving SFR is verified. Second, a slightly increased total cost improves the system's dynamic performance. Third, the increased charging time is secured with the proposed charging time constraints.

V. CONCLUSION

In conclusion, this paper proposes an EV charging time-constrained deliverable SFR provision model. First, the state space modeling addresses the uncertainties from EV heterogeneous parameters and traveling behaviors. The EV owner's preference translation respects the charging time into a real-time AGC activation limiter for the individual EV. Second, estimating EV SFR capacities facilitates inter-interval SFR reserve procurement, and the EV aggregation strategy reliably delivers real-time intra-interval AGC response. Third, a hybrid OPF structure is proposed in the RTED-TDS cosimulation to evaluate the economic and reliability performance of EV aggregation's SFR provision. The proposed structure can secure the broadcasting dispatch results into the dynamic simulation, reducing the overall cosimulation modeling complexity. Last, the proposed charging time-constrained EV aggregation is verified using the RTED-TDS cosimulation framework on IEEE 39-bus system. Results indicate that the proposed model can improve the system's dynamic performance and respect the EV owners' tolerance of increased charging time.

ACKNOWLEDGMENT

The views expressed in the article do not necessarily represent the views of the DOE or the U.S. Government. The U.S. Government retains and the publisher, by accepting the article for publication, acknowledges that the U.S. Government retains a nonexclusive, paid-up, irrevocable, worldwide license to publish or reproduce the published form of this work, or allow others to do so, for U.S. Government purposes.

REFERENCES

[1] (North Amer. Electric Rel. Corp., Atlanta, GA, USA). *Ancillary Service and Balancing Authority Area Solutions to Integrate Variable Generation*. 2011. [Online]. Available: https://www.nerc.com/pa/RAPA/ra/Reliability

[2] N. Gao, D. W. Gao, and X. Fang, "Manage real-time power imbalance with renewable energy: Fast generation dispatch or adaptive frequency regulation?," *IEEE Trans. Power Syst.*, vol. 38, no. 6, pp. 5278–5289, Nov. 2023. [Online]. Available: https://ieeexplore.ieee.org/document/10002304/

[3] X. Fang, B.-M. Hodge, L. Bai, H. Cui, and F. Li, "Mean-variance optimization-based energy storage scheduling considering day-ahead and real-time LMP uncertainties," *IEEE Trans. Power Syst.*, vol. 33, no. 6, pp. 7292–7295, Nov. 2018. [Online]. Available: https://ieeexplore.ieee.org/document/8409961/

[4] H. Cui, F. Li, X. Fang, H. Chen, and H. Wang, "Bilevel arbitrage potential evaluation for grid-scale energy storage considering wind power and LMP smoothing effect," *IEEE Trans. Sustain. Energy*, vol. 9, no. 2, pp. 707–718, Apr. 2018. [Online]. Available: http://ieeexplore.ieee.org/document/8057838/

[5] C. Ning and F. You, "Data-driven adaptive robust unit commitment under wind power uncertainty: A Bayesian nonparametric approach," *IEEE Trans. Power Syst.*, vol. 34, no. 3, pp. 2409–2418, May 2019. [Online]. Available: https://ieeexplore.ieee.org/document/8603781/

[6] G. Zhang, E. Ela, and Q. Wang, "Market scheduling and pricing for primary and secondary frequency reserve," *IEEE Trans. Power Syst.*, vol. 34, no. 4, pp. 2914–2924, Jul. 2019. [Online]. Available: https://ieeexplore.ieee.org/document/8585108/

[7] X. Fang, H. Yuan, and J. Tan, "Secondary frequency regulation from variable generation through uncertainty decomposition: An economic and reliability perspective," *IEEE Trans. Sustain. Energy*, vol. 12, no. 4, pp. 2019–2030, Oct. 2021. [Online]. Available: https://ieeexplore.ieee.org/document/9420286/

[8] W. Kempton and J. Tomić, "Vehicle-to-grid power implementation: From stabilizing the grid to supporting large-scale renewable energy," *J. Power Sources*, vol. 144, no. 1, pp. 280–294, 2005. [Online]. Available: https://linkinghub.elsevier.com/retrieve/pii/S0378775305000212

[9] C. Liu, K. T. Chau, D. Wu, and S. Gao, "Opportunities and challenges of vehicle-to-home, vehicle-to-vehicle, and vehicle-to-grid technologies," *Proc. IEEE*, vol. 101, no. 11, pp. 2409–2427, Nov. 2013. [Online]. Available: http://ieeexplore.ieee.org/document/6571224/

[10] E. Sortomme and M. A. El-Sharkawi, "Optimal scheduling of vehicle-to-grid energy and ancillary services," *IEEE Trans. Smart Grid*, vol. 3, no. 1, pp. 351–359, Mar. 2012. [Online]. Available: http://ieeexplore.ieee.org/document/6021358/

[11] M. G. Vaya and G. Andersson, "Self scheduling of plug-in electric vehicle aggregator to provide balancing services for wind power," *IEEE Trans. Sustain. Energy*, vol. 7, no. 2, pp. 886–899, Apr. 2016. [Online]. Available: http://ieeexplore.ieee.org/document/7345600/

[12] K. Kaur, M. Singh, and N. Kumar, "Multiobjective optimization for frequency support using electric vehicles: An aggregator-based hierarchical control mechanism," *IEEE Syst. J.*, vol. 13, no. 1, pp. 771–782, Mar. 2019. [Online]. Available: https://ieeexplore.ieee.org/document/8121976/

[13] L. Argiolas, M. Stecca, L. M. Ramirez-Elizondo, T. B. Soeiro, and P. Bauer, "Optimal battery energy storage dispatch in energy and frequency regulation markets while peak shaving an EV fast charging station," *IEEE Open Access J. Power Energy*, vol. 9, pp. 374–385, 2022. [Online]. Available: https://ieeexplore.ieee.org/document/9855507/

[14] B. Wang, P. Dehghanian, and D. Zhao, "Coordinated planning of electric vehicle charging infrastructure and renewables in power grids," *IEEE Open Access J. Power Energy*, vol. 10, pp. 233–244, 2023. [Online]. Available: https://ieeexplore.ieee.org/document/10045673/

[15] S. Cai and R. Matsuhashi, "Optimal dispatching control of EV aggregators for load frequency control with high efficiency of EV utilization," *Appl. Energy*, vol. 319, Aug. 2022, Art. no. 119233. [Online]. Available: https://linkinghub.elsevier.com/retrieve/pii/S0306261922005955

[16] M. Wang et al., "State space model of aggregated electric vehicles for frequency regulation," vol. 11, no. 2, pp. 981–994, Mar. 2020. [Online]. Available: https://ieeexplore.ieee.org/document/8764460/

[17] S. Kiani, K. Sheshyekani, and H. Dagdougui, "An extended state space model for aggregation of large-scale EVs considering fast charging," *IEEE Trans. Transp. Electrific.*, vol. 9, no. 1, pp. 1238–1251, Mar. 2023. [Online]. Available: https://ieeexplore.ieee.org/document/9785801/

[18] T. Kerci and F. Milano, "A framework to embed the unit commitment problem into time domain simulations," in *Proc. IEEE Int. Conf. Environ. Electr. Eng. IEEE Ind. Commer. Power Syst. Eur.*, 2019, pp. 1–5. [Online]. Available: https://ieeexplore.ieee.org/document/8783983/

[19] T. Kerci, M. A. A. Murad, I. Dassios, and F. Milano, "On the impact of discrete secondary controllers on power system dynamics," *IEEE Trans. Power Syst.*, vol. 36, no. 5, pp. 4400–4409, Sep. 2021. [Online]. Available: https://ieeexplore.ieee.org/document/9361269/

[20] D. Knutsen and O. Willén, "A study of electric vehicle charging patterns and range anxiety," Dept. Eng. Sci., Uppsala Univ., Uppsala, Sweden, Rep. UPTEC STS13 015, Jun. 2013. [Online]. Available: http://www.diva-portal.org/smash/record.jsf?pid=diva2%3A626048&dswid=516

[21] A. Alsabbagh, B. Wu, and C. Ma, "Distributed electric vehicles charging management considering time anxiety and customer behaviors," *IEEE Trans. Ind. Informat.*, vol. 17, no. 4, pp. 2422–2431, Apr. 2021. [Online]. Available: https://ieeexplore.ieee.org/document/9121753/

[22] L. Yan, X. Chen, J. Zhou, Y. Chen, and J. Wen, "Deep reinforcement learning for continuous electric vehicles charging control with dynamic user behaviors," *IEEE Trans. Smart Grid*,vol. 12, no. 6, pp. 5124–5134, Nov. 2021. [Online]. Available: https://ieeexplore.ieee.org/document/9493711/

[23] B. Wang, D. Zhao, P. Dehghanian, Y. Tian, and T. Hong, "Aggregated electric vehicle load modeling in large-scale electric power systems," *IEEE Trans. Ind. Appl.*, vol. 56, no. 5, pp. 5796–5810, Sep./Oct. 2020. [Online]. Available: https://ieeexplore.ieee.org/document/9069450/

[24] Q. Shi, H. Cui, F. Li, Y. Liu, W. Ju, and Y. Sun, "A hybrid dynamic demand control strategy for power system frequency regulation," *CSEE J. Power Energy Syst.*, vol. 3, no. 2, pp. 176–185, Jun. 2017. [Online]. Available: https://ieeexplore.ieee.org/stamp/stamp.jsp?tp=arnumber=7976165

[25] L. Thurner et al., "Pandapower—an open-source python tool for convenient modeling, analysis, and optimization of electric power systems," *IEEE Trans. Power Syst.*, vol. 33, no. 6, pp. 6510–6521, Nov. 2018. [Online]. Available: https://ieeexplore.ieee.org/document/8344496/

[26] H. Cui, F. Li, and K. Tomsovic, "Hybrid symbolic-numeric framework for power system modeling and analysis," *IEEE Trans. Power Syst.*, vol. 36, no. 2, pp. 1373–1384, Mar. 2021. [Online]. Available: https://ieeexplore.ieee.org/document/9169830/

[27] F. Li, K. Tomsovic, and H. Cui, "A large-scale testbed as a virtual power grid: For closed-loop controls in research and testing," *IEEE Power Energy Mag.*, vol. 18, no. 2, pp. 60–68, Mar./Apr. 2020. [Online]. Available: https://ieeexplore.ieee.org/document/9007798/

[28] W. Wang, X. Fang, H. Cui, F. Li, Y. Liu, and T. J. Overbye, "Transmission-and-distribution dynamic co-simulation framework for distributed energy resource frequency response," *IEEE Trans. Smart Grid*, vol. 13, no. 1, pp. 482–495, Jan. 2022. [Online]. Available: https://ieeexplore.ieee.org/document/9569771/

[29] "Data miner 2." PJM.com. Accessed: May 28, 2022. [Online]. Available: https://dataminer2.pjm.com/list

[30] N. Parsly, J. Wang, N. West, Q. Zhang, H. Cui, and F. Li, "DiME and AGVis: A distributed messaging environment and geographical visualizer for large-scale power system simulation," in *Proc. North Amer. Power Symp. (NAPS)*, 2023, pp. 1–5. [Online]. Available: https://ieeexplore.ieee.org/document/10318583/

[31] J. Li, J. Wen, and X. Han, "Low-carbon unit commitment with intensive wind power generation and carbon capture power plant," *J. Modern Power Syst. Clean Energy*, vol. 3, no. 1, pp. 63–71, Mar. 2015. [Online]. Available: http://link.springer.com/10.1007/s40565-014-0095-6

[32] C. M. Adrah, D. Palma, O. Kure, and P. E. Heegaard, "Deploying 5g architecture for protection systems in smart distribution grids," in *Proc. IEEE Power Energy Soc. Innov. Smart Grid Technol. Conf. (ISGT)*, 2022, pp. 1–5. [Online]. Available: https://ieeexplore.ieee.org/document/9817536/

Jinning Wang (Graduate Student Member, IEEE) received the B.S. and M.S. degrees in electrical engineering from the Taiyuan University of Technology, Taiyuan, China, in 2017 and 2020, respectively. He is currently pursuing the Ph.D. degree in electrical engineering with The University of Tennessee, Knoxville, TN, USA. His research interests include data mining, scientific computation, and power system simulation.

Fangxing Li (Fellow, IEEE) is also known as Fran Li. He received the B.S.E.E. and M.S.E.E. degrees from Southeast University, Nanjing, China, in 1994 and 1997, respectively, and the Ph.D. degree from Virginia Tech, Blacksburg, VA, USA, in 2001.

He is currently the John W. Fisher Professor of Electrical Engineering and the Campus Director of CURENT, The University of Tennessee, Knoxville, TN, USA. His current research interests include resilience, artificial intelligence in power, demand response, distributed generation and microgrid, and energy markets. He has received numerous awards and honors including R&D 100 Award in 2020, IEEE PES Technical Committee Prize Paper Award in 2019, five best or prize paper awards at international journals, and six best papers/posters at international conferences. From 2020 to 2021, he served as the Chair of IEEE PES Power System Operation, Planning and Economics Committee. He has been serving as the Chair of IEEE WG on Machine Learning for Power Systems since 2019 and has been the Editor-In-Chief of IEEE OPEN ACCESS JOURNAL OF POWER AND ENERGY since 2020.

Xin Fang (Senior Member, IEEE) received the B.S. degree from the Huazhong University of Science and Technology, Wuhan, China, in 2009, the M.S. degree from China Electric Power Research Institute. Beijing, China, in 2012, and the Ph.D. degree from The University of Tennessee, Knoxville, TN, USA, in 2016.

He is currently an Assistant Professor with the Department of Electrical and Computer Engineering, Mississippi State University (MSU). Before joining MSU, he was a Senior Researcher with National Renewable Energy Laboratory from 2017 to 2022. His research interests include power system planning and operation, electricity market operation considering renewable energy integration, and cyber-physical transmission and distribution modeling and simulation. He is an Associate Editor of IEEE TRANSACTIONS ON POWER SYSTEMS and IEEE TRANSACTIONS ON SUSTAINABLE ENERGY.

Wenbo Wang (Member, IEEE) received the M.Sc. and Ph.D. degrees in electrical engineering from the Tandon School of Engineering, New York University in 2015 and 2019, respectively. He is currently a Researcher with National Renewable Energy Laboratory. His research interests include distribution system modeling and analysis, transmission and distribution cosimulation, dynamic thermal rating, and data-driven methods in power systems.

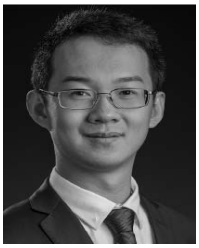

Hantao Cui (Senior Member, IEEE) received the B.S. and M.S. degrees in electrical engineering from Southeast University, China, and the Ph.D. degree in electrical engineering from The University of Tennessee, Knoxville, in 2018. He is currently an Assistant Professor with the School of Electrical and Computer Engineering, Oklahoma State University. His research interests include power system modeling, simulation, and high-performance computing. He is a winner of the 2024 NSF CAREER Award. He was the Chief Technologist of the CURENT Large Scale Testbed, which won the 2020 R&D 100 Awards.

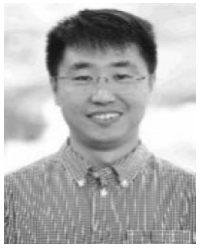

Qiwei Zhang (Member, IEEE) received the M.S. and Ph.D. degrees in electrical engineering from The University of Tennessee, Knoxville, in 2018 and 2022, respectively. He is currently a Postdoctoral Research Fellow with Johns Hopkins University. Prior to this, he was a Research Scientist with The University of Tennessee. His research interests include renewable integration, power system cybersecurity, and electricity market.

Buxin She (Member, IEEE) received the B.S.E.E. and M.S.E.E. degrees in electrical engineering from Tianjin University, China, in 2017 and 2019, respectively, and the Ph.D. degree in electrical engineering from the University of Tennessee, Knoxville, in 2023. He is currently a Research Engineer with Pacific Northwest National Laboratory. His research interests include microgrid operation and control, machine learning in power systems, distribution system operation and plan, and power grid resilience. He served as a Student Guest Editor of *IET Renewable Power Generation*. He was an outstanding Reviewer of IEEE OPEN ACCESS JOURNAL OF POWER AND ENERGY and *Journal of Modern Power System and Clean Energy*.